Figure captions

Fig. 1: Map of the geographic distribution of the maximum variation of vertical wind speed (m/s) across the vertical dimension of the simulated domain (10-120 hPa) on July 17th, 2006 at 12:00UTC.

Fig. 2: Vertical profiles of vertical wind speed *w* (left, m/s) and temperature (right, K) for the two points identified as being affected by intense (blue line) or no GW activity (green line) in Fig. 1.

Fig. 3: Vertical, zonal cross-sections of vertical wind speed (left, m/s) and temperature (right, K) as a function of longitude and pressure for latitude near 70°S on July 17th, 2006 at 12:00UTC.

Fig. 4: Frequency of domain grid cells being affected by GW events during June-July-August 2006-2010.

Fig. 5: Frequency of GW affecting cell domains as a function of longitude.

Fig. 6: Distributions of absolute vertical wind speeds faster than 1 m/s above the simulation domain (10-120hPa) as a function of time, for each Antarctic summer between 2006 and 2010. Note that no simulation was run before June 13, 2006 (date of first available CALIOP data).

Fig. 7: Same as Fig. 6, for temperature (K) instead of wind speed.

Fig. 8: Evolution of PSC volume per profile during the 2006 (top), 2008 (middle) and 2009 (bottom) Antarctic winter seasons, for ice (blue) and NAT (green) PSC. Thick lines indicate periods identified as GW events following Table 1. Shaded regions indicate undersampled periods (e.g. missing CALIOP observations).

Fig. 9: Distribution of daily PSC volume per profile for PSC identified as ice (top) and NAT (bottom), for all seasons (left column), during GW events (middle) and calm periods (right)

Fig. 10: Evolution of the volume per profile of ice and NAT PSC as a function of time after the end of GW events.

Fig. 11: Volume of ice (blue, thin) and NAT (green, thick) PSC during GW events (top) and calm periods (bottom), averaged per profile, as a function of longitude in 10° bins. Note that the range of the vertical axis for NAT PSC volume is double the one for ice PSC.

Fig. 12: time series of water vapor mixing ratios profiles observed by MLS and averaged daily over the simulation domain for the 2006 winter season. The gap near July 10 is due to missing data.

Fig. 13: Same as Fig. 12, for ice frost point profiles retrieved from the daily averaged MLS water vapor mixing ratios shown in Fig. 12.

Fig. 14: Evolution of daily domain volume with temperatures colder than the ice frost point Tice for 2006, 2008 and 2009 Antarctic winters. GW events described in Sect. 2 are identified by thick lines.

Fig. 15: distributions of daily volumes with temperatures colder than the ice frost point Tice, during GW events (left) and calm periods (right).

Fig. 16: Simultaneous evolution during the 2006 Antarctic winter of volumes with stratospheric temperatures below the ice frost point (line) and volumes of ice PSC (dots), from the intersection of WRF model output with CALIOP observations.

Fig. 17: Histogram of observed ice PSC volume vs. volumes with temperatures conducive to ice PSC formation

Fig. 18: Ratio of the observed volume of PSC on the modeled volume of temperatures conducive to PSC formation, for ice PSC (blue) and NAT PSC (green), considering all periods (full line) and GW events (dashed lines).

Fig. 19: Ratio of the observed volume of NAT PSC on the modeled volume of temperatures conducive to NAT PSC formation, for four ranges of observed ice PSC volumes, as a function of the delay after ice PSC observation. Volumes were aggregated over 36-hours periods with an adjustable delay between ice and NAT data.

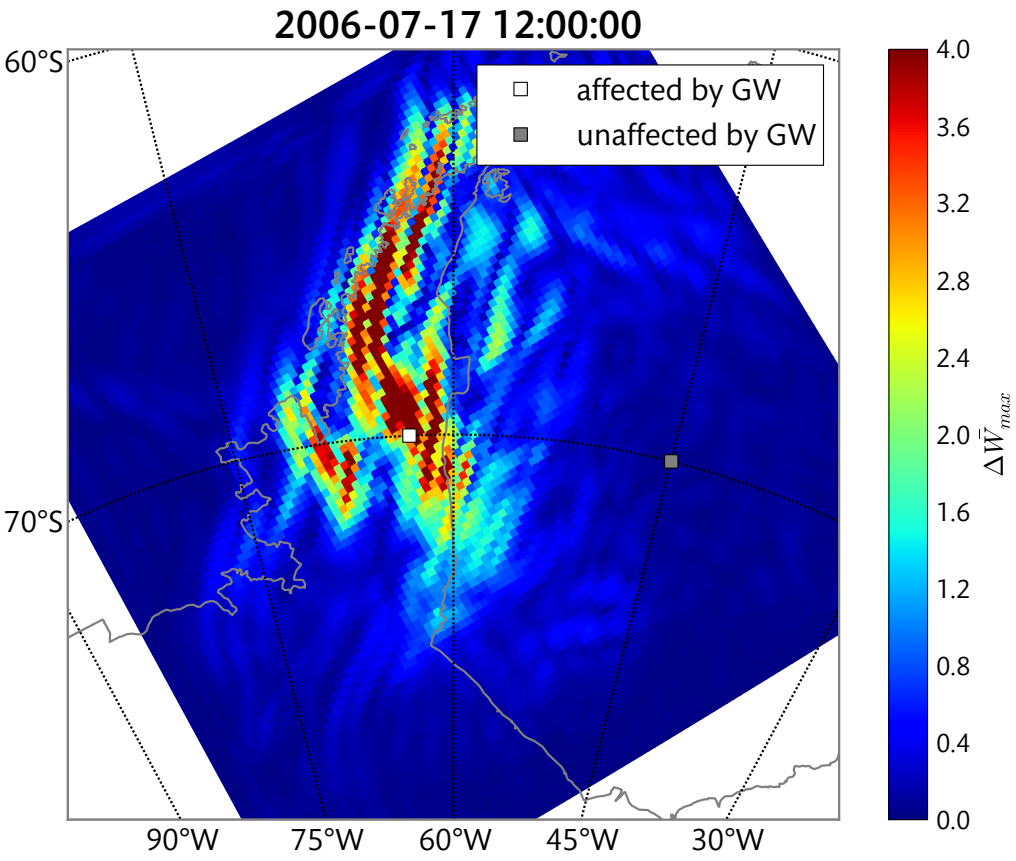

Fig. 1: Map of the geographic distribution of the maximum variation of vertical wind speed (m/s) across the vertical dimension of the simulated domain (10-120 hPa) on July 17th, 2006 at 12:00UTC.

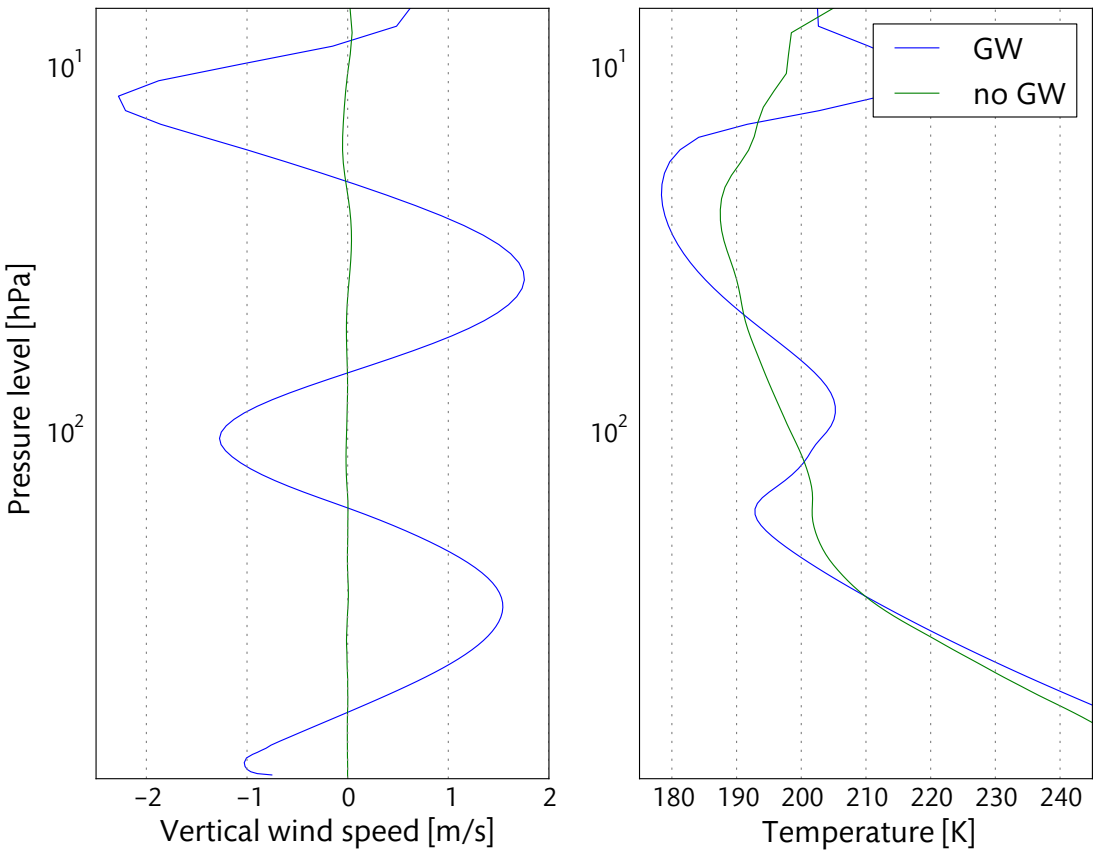

Fig. 2: Vertical profiles of vertical wind speed *w* (left, m/s) and temperature (right, K) for the two points identified as being affected by intense (blue line) or no GW activity (green line) in Fig. 1.

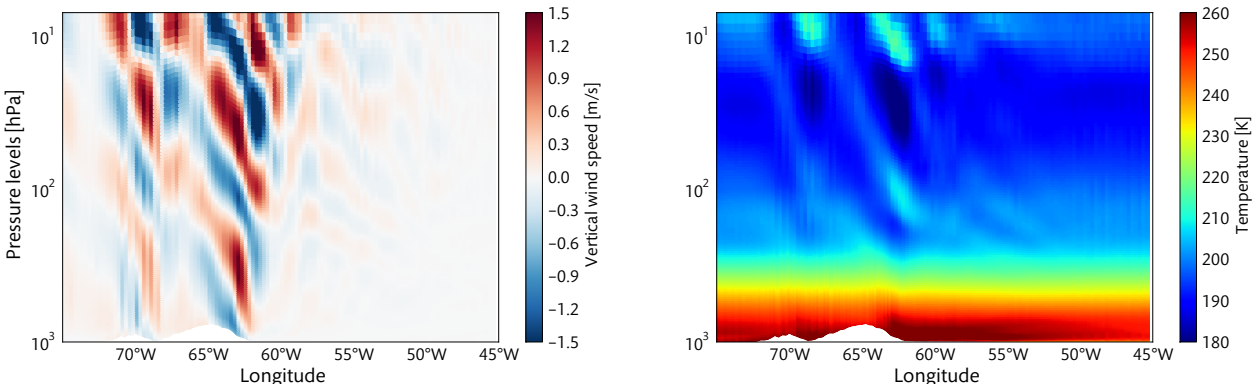

Fig. 3: Vertical, zonal cross-sections of vertical wind speed (left, m/s) and temperature (right, K) as a function of longitude and pressure for latitude near 70°S on July 17th, 2006 at 12:00UTC.

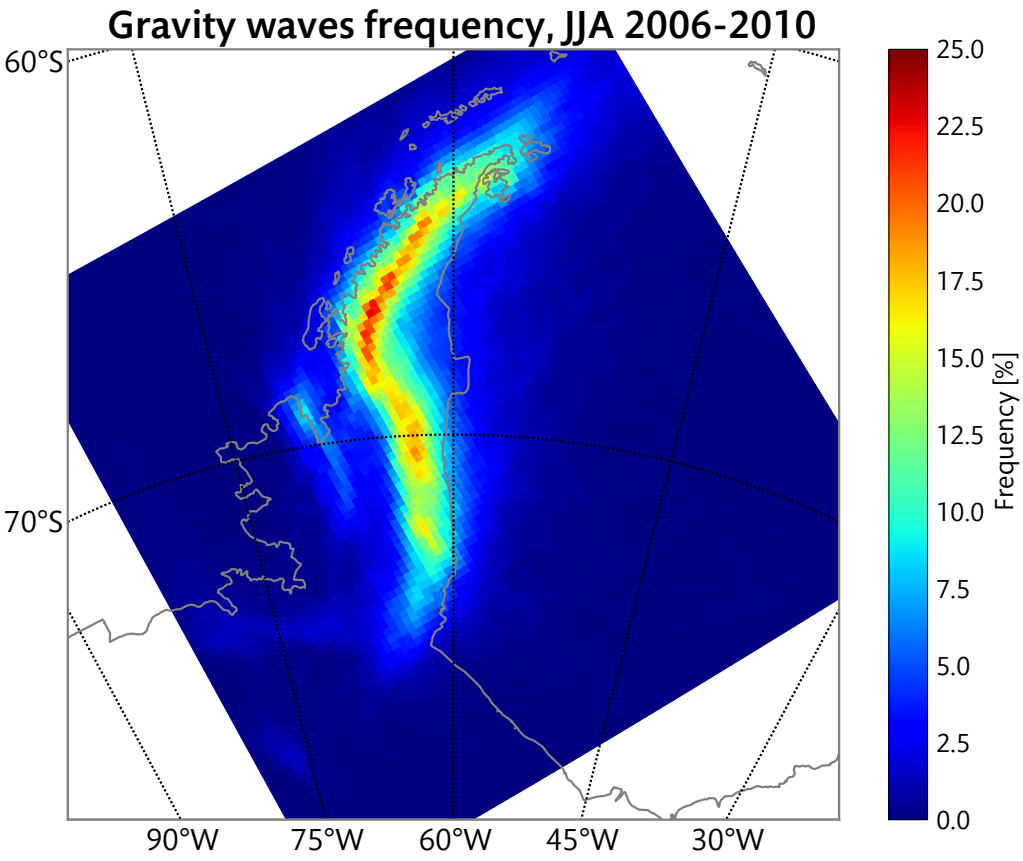

Fig. 4: Frequency of domain grid cells being affected by GW events during June-July-August 2006-2010.

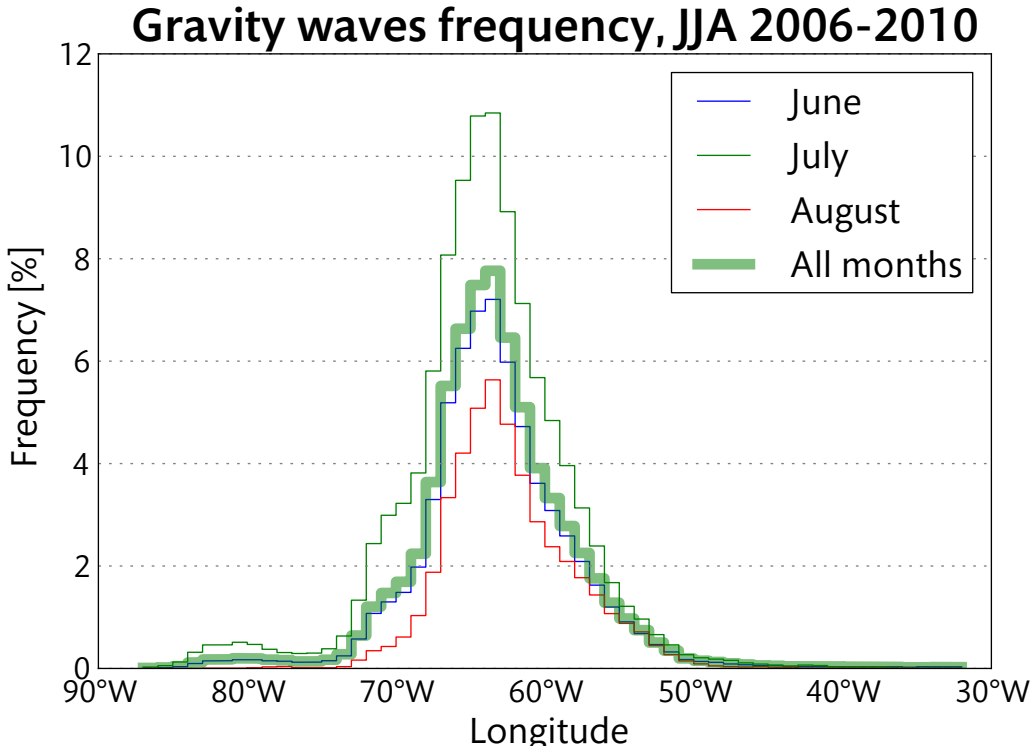

Fig. 5: Frequency of GW affecting cell domains as a function of longitude.

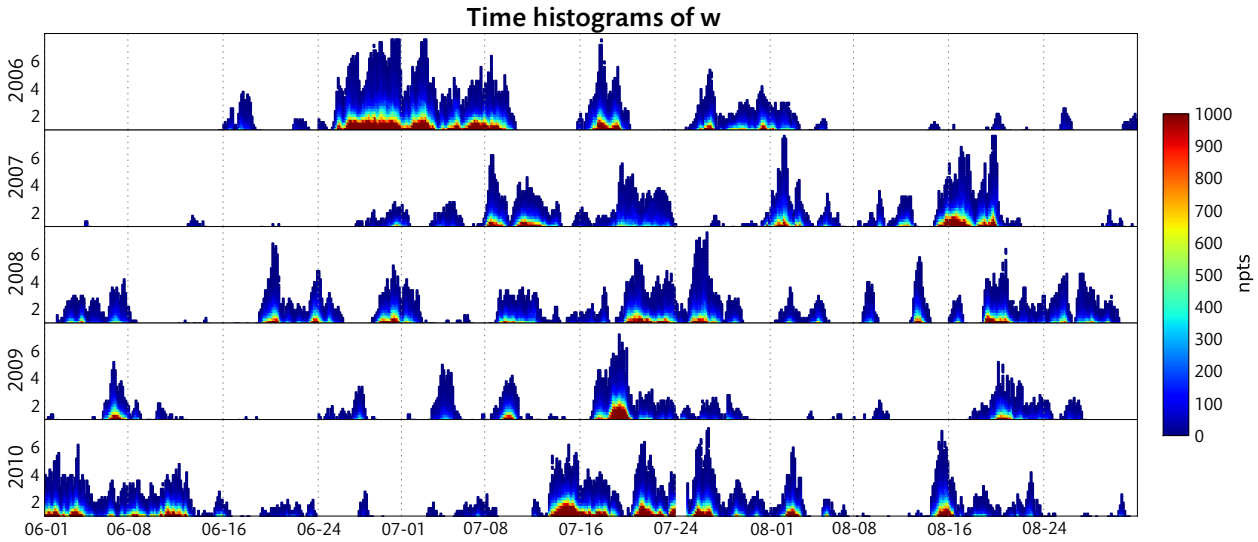

Fig. 6: Distributions of absolute vertical wind speeds faster than 1 m/s above the simulation domain (10-120hPa) as a function of time, for each Antarctic summer between 2006 and 2010. Note that no simulation was run before June 13, 2006 (date of first available CALIOP data).

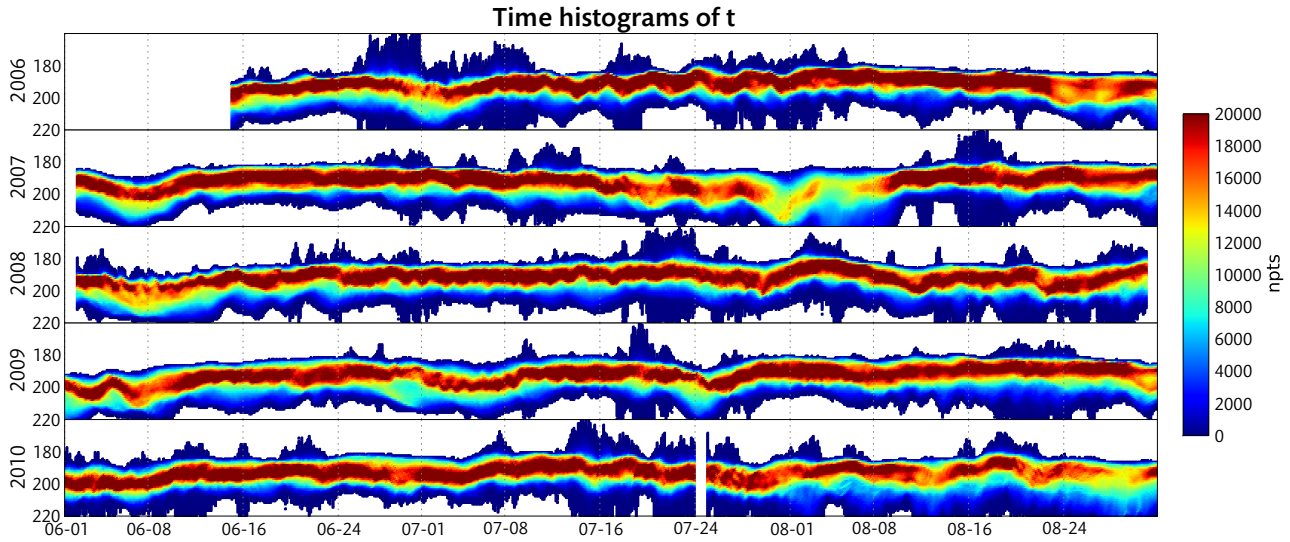

Fig. 7: Same as Fig. 6, for temperature (K) instead of wind speed.

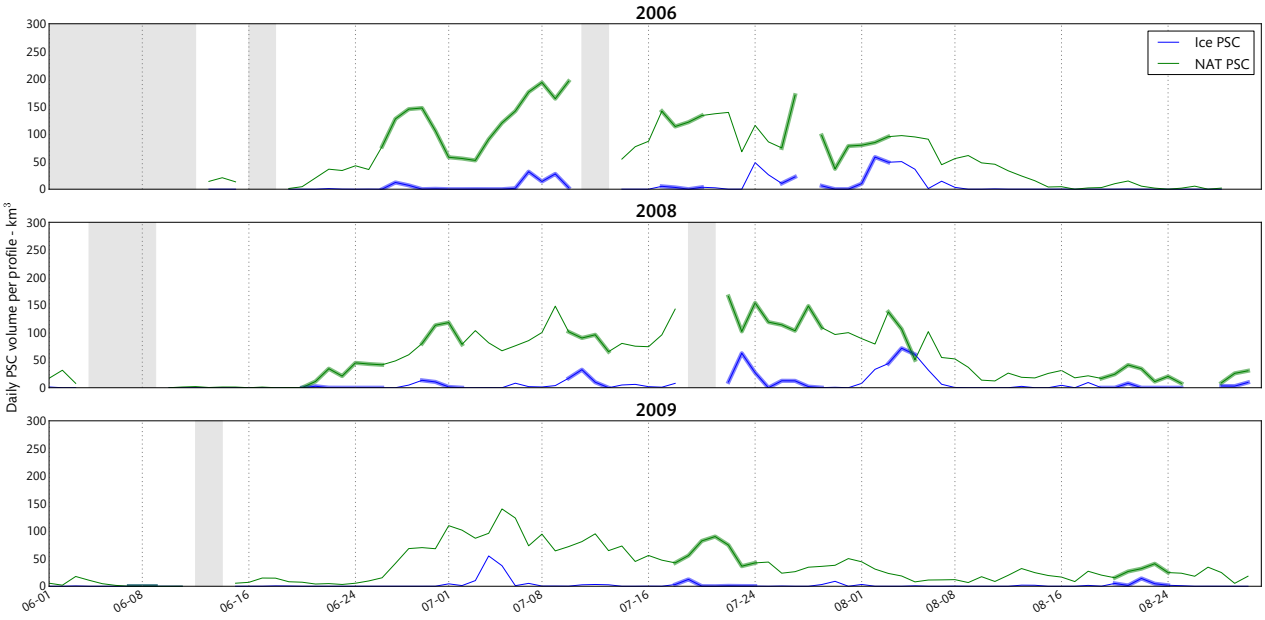

Fig. 8: Evolution of PSC volume per profile during the 2006 (top), 2008 (middle) and 2009 (bottom) Antarctic winter seasons, for ice (blue) and NAT (green) PSC. Thick lines indicate periods identified as GW events following Table 1. Shaded regions indicate undersampled periods (e.g. missing CALIOP observations).

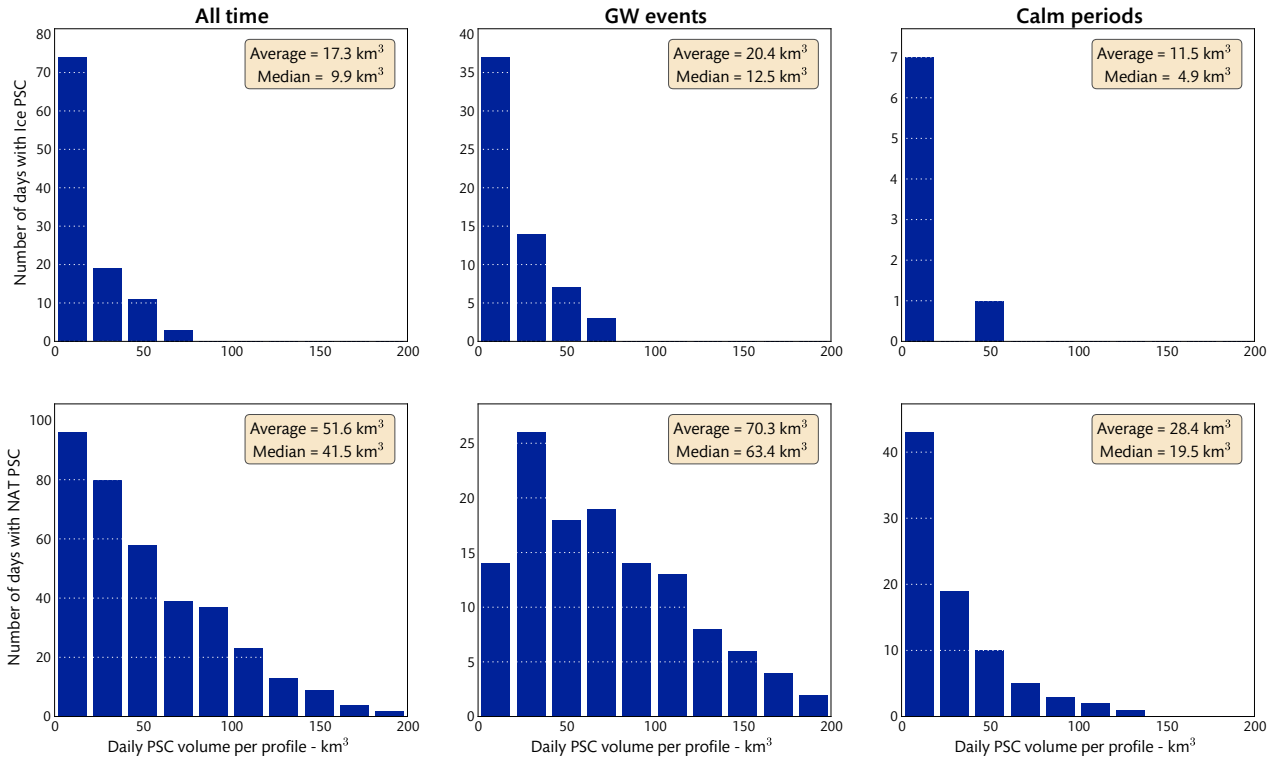

Fig. 9: Distribution of daily PSC volume per profile for PSC identified as ice (top) and NAT (bottom), for all seasons (left column), during GW events (middle) and calm periods (right)

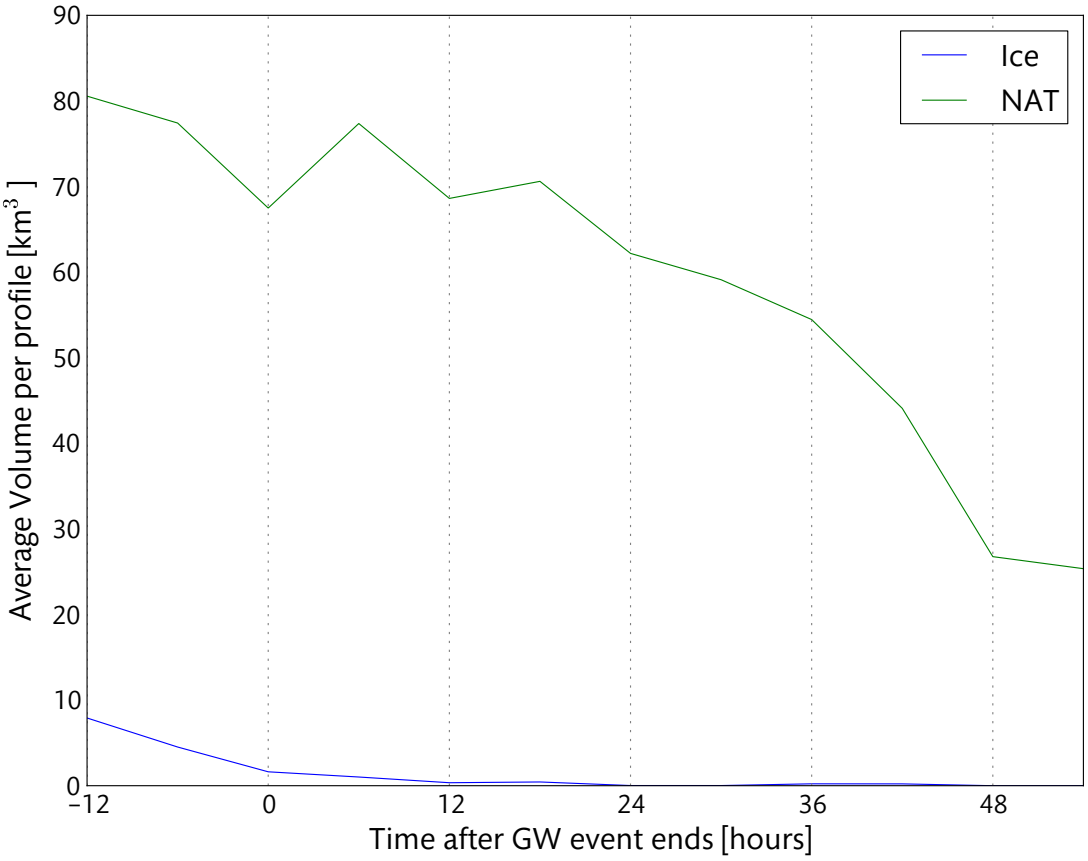

Fig. 10: Evolution of the volume per profile of ice and NAT PSC as a function of time after the end of GW events.

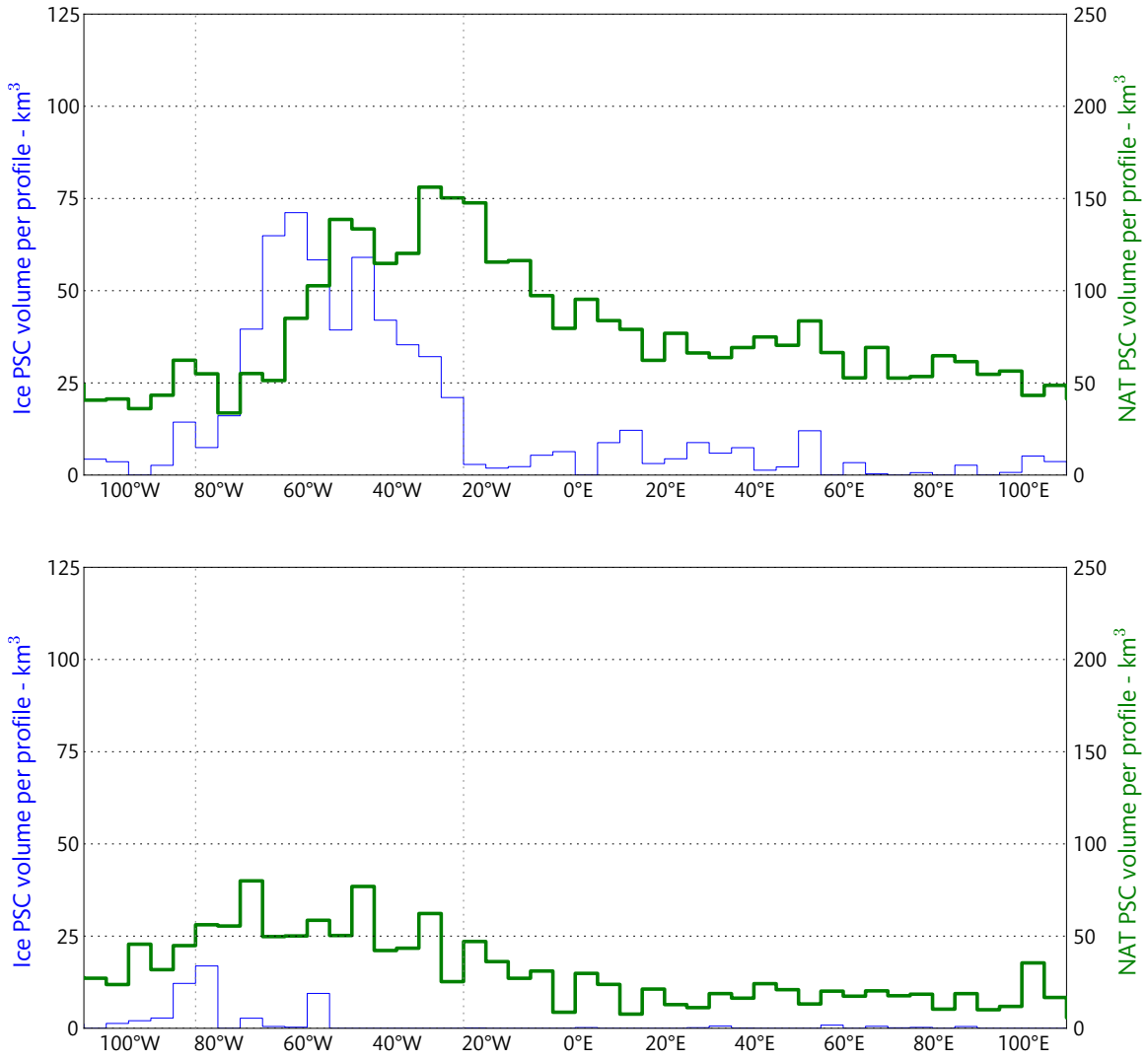

Fig. 11: Volume of ice (blue, thin) and NAT (green, thick) PSC during GW events (top) and calm periods (bottom), averaged per profile, as a function of longitude in 10° bins. Note that the range of the vertical axis for NAT PSC volume is double the one for ice PSC.

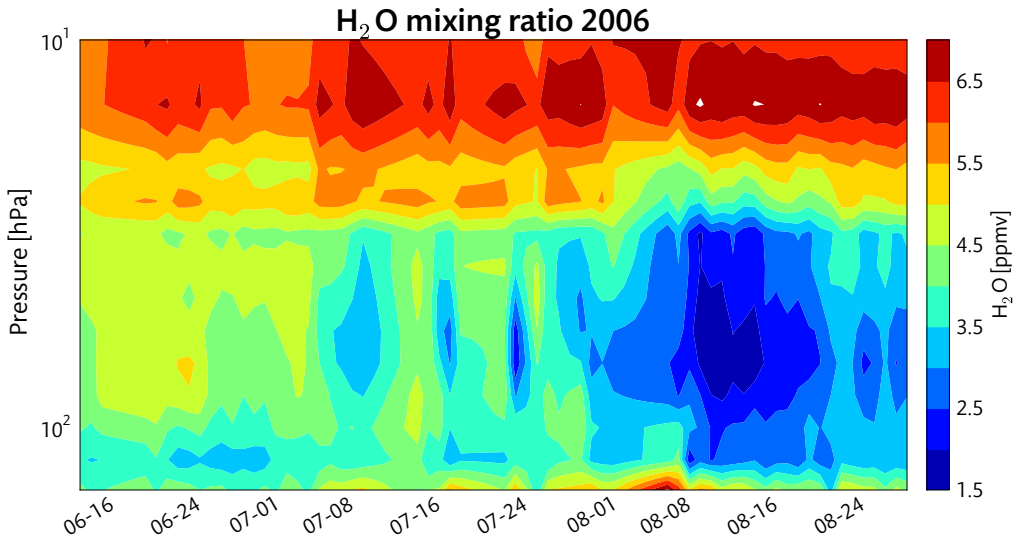

Fig. 12: time series of water vapor mixing ratios profiles observed by MLS and averaged daily over the simulation domain for the 2006 winter season. The gap near July 10 is due to missing data.

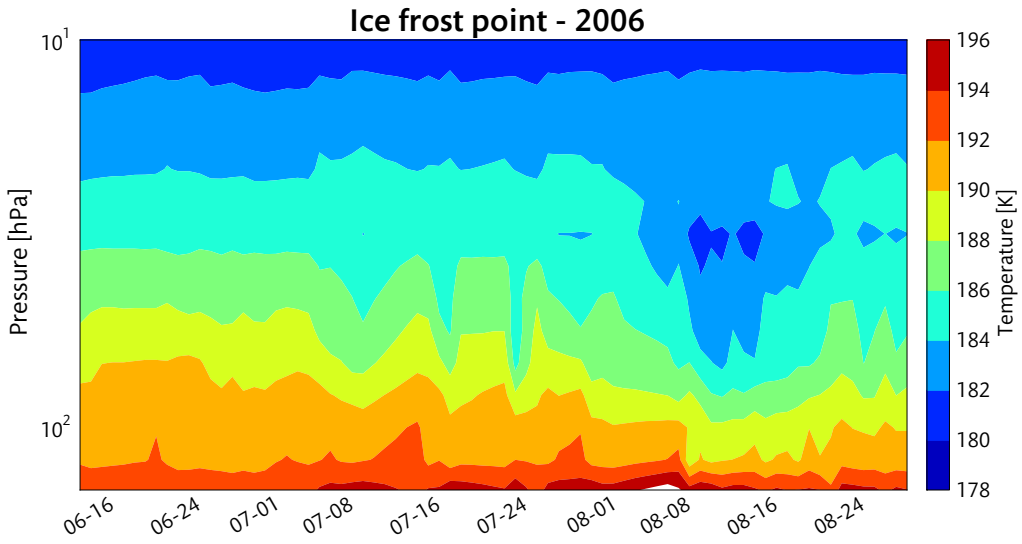

Fig. 13: Same as Fig. 12, for ice frost point profiles retrieved from the daily averaged MLS water vapor mixing ratios shown in Fig. 12.

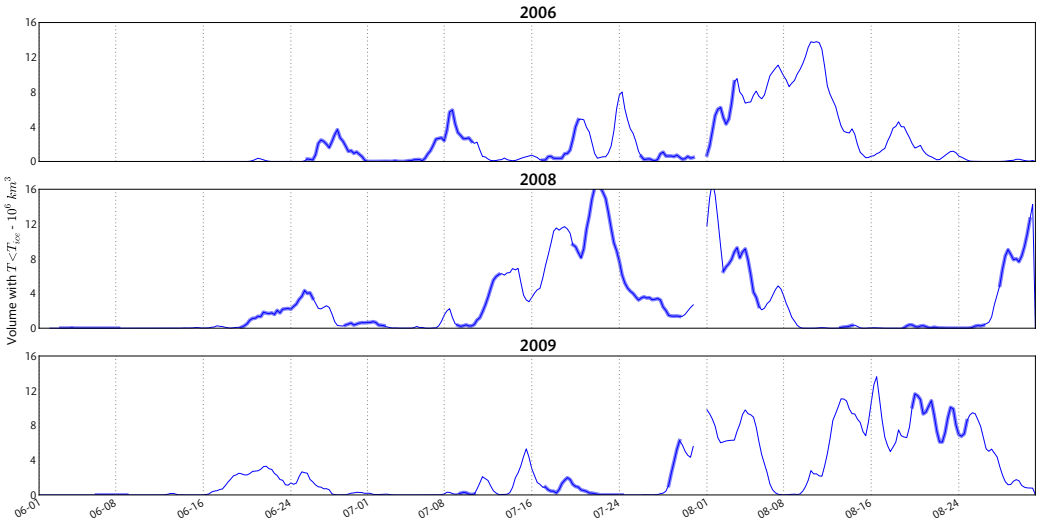

Fig. 14: Evolution of daily domain volume with temperatures colder than the ice frost point Tice for 2006, 2008 and 2009 Antarctic winters. GW events described in Sect. 2 are identified by thick lines.

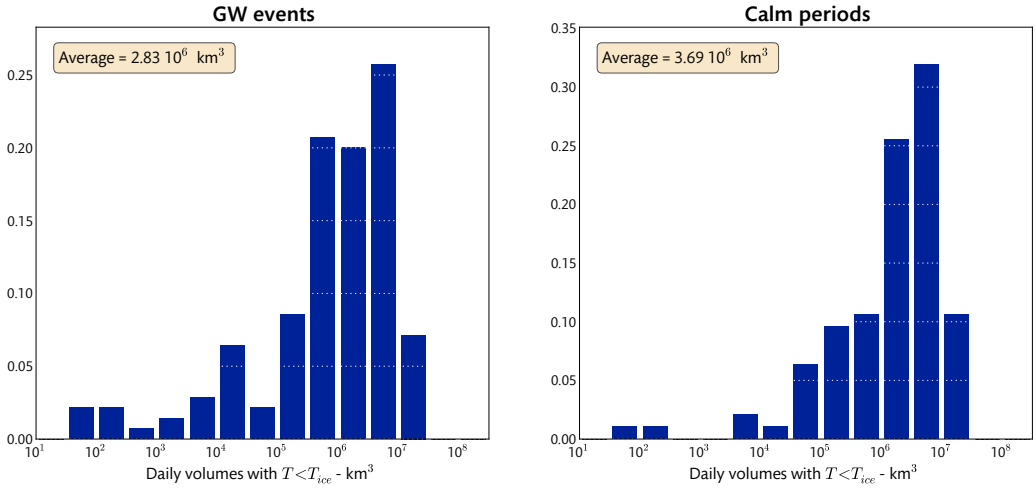

Fig. 15: distributions of daily volumes with temperatures colder than the ice frost point Tice, during GW events (left) and calm periods (right).

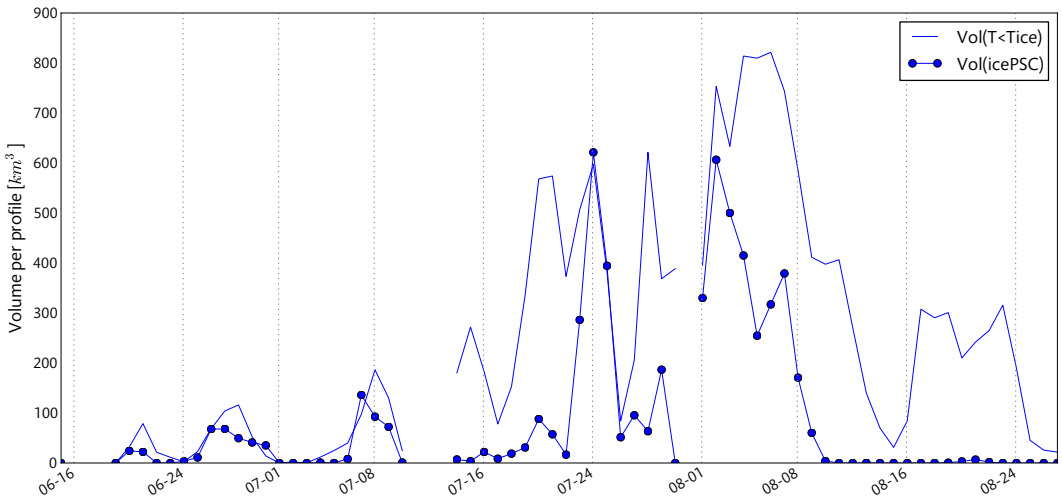

Fig. 16: Simultaneous evolution during the 2006 Antarctic winter of volumes with stratospheric temperatures below the ice frost point (line) and volumes of ice PSC (dots), from the intersection of WRF model output with CALIOP observations.

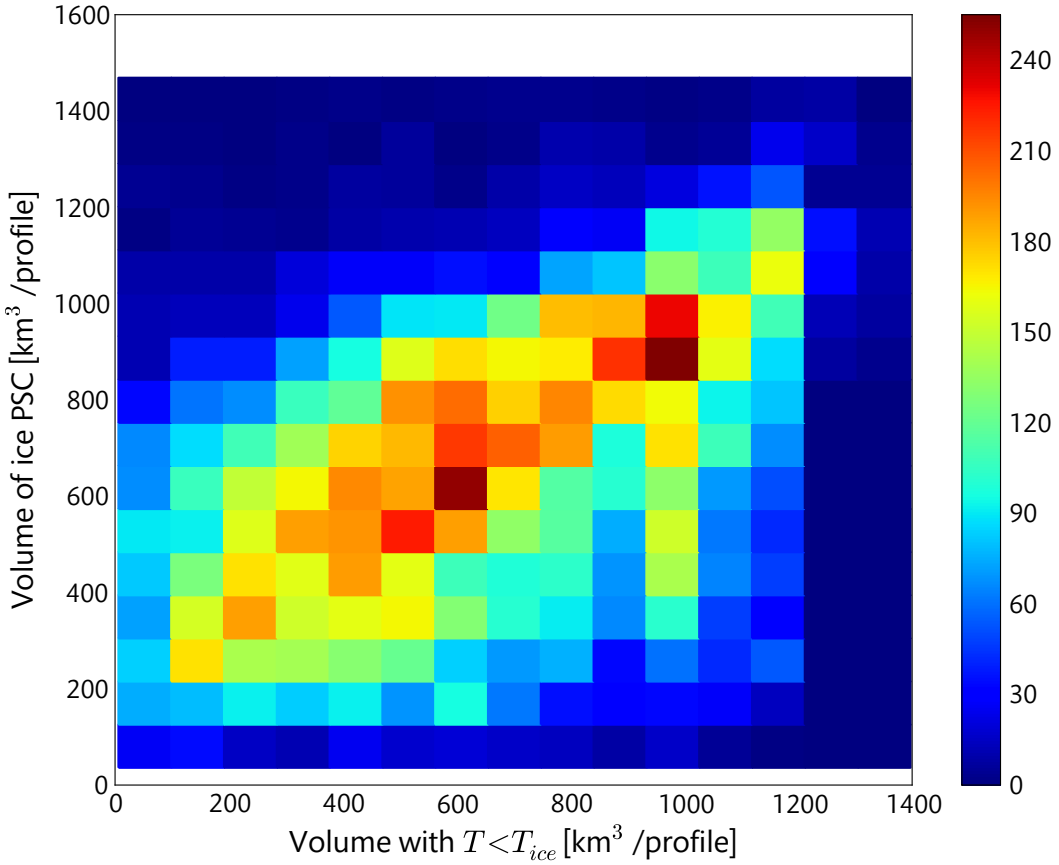

Fig. 17: Histogram of observed ice PSC volume vs. volumes with temperatures conducive to ice PSC formation

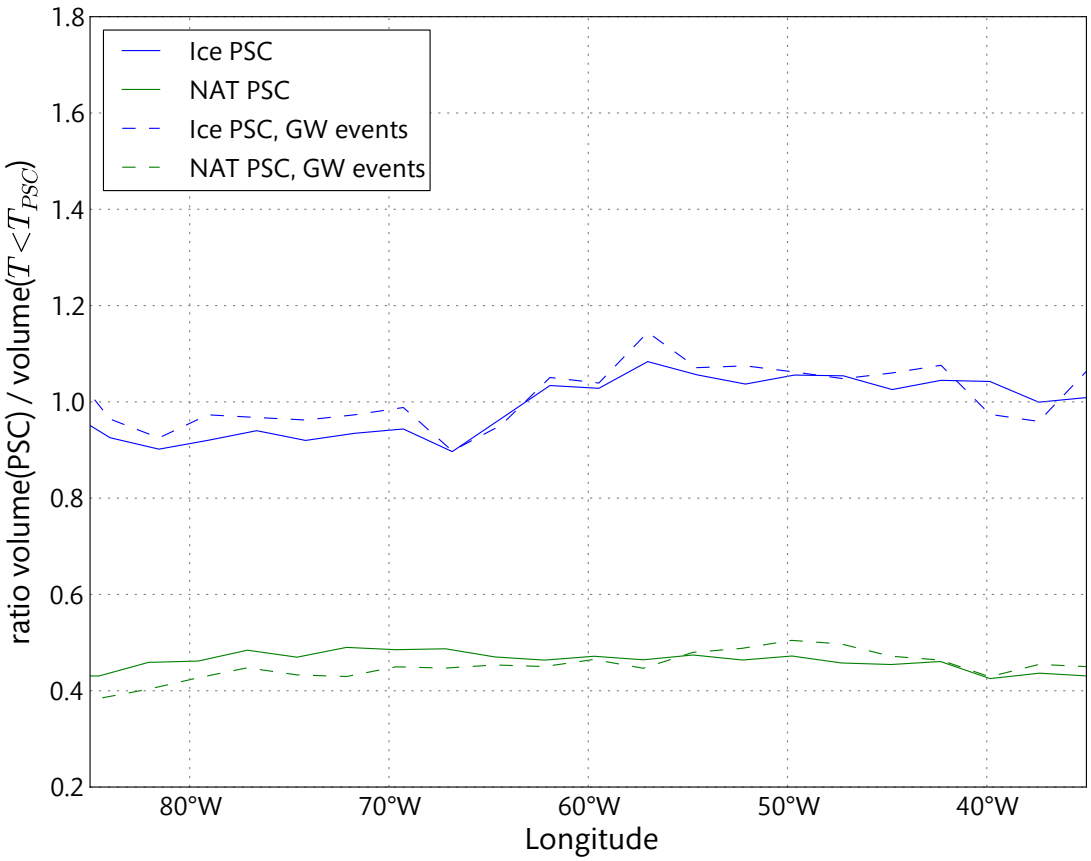

Fig. 18: Ratio of the observed volume of PSC on the modeled volume of temperatures conducive to PSC formation, for ice PSC (blue) and NAT PSC (green), considering all periods (full line) and GW events (dashed lines).

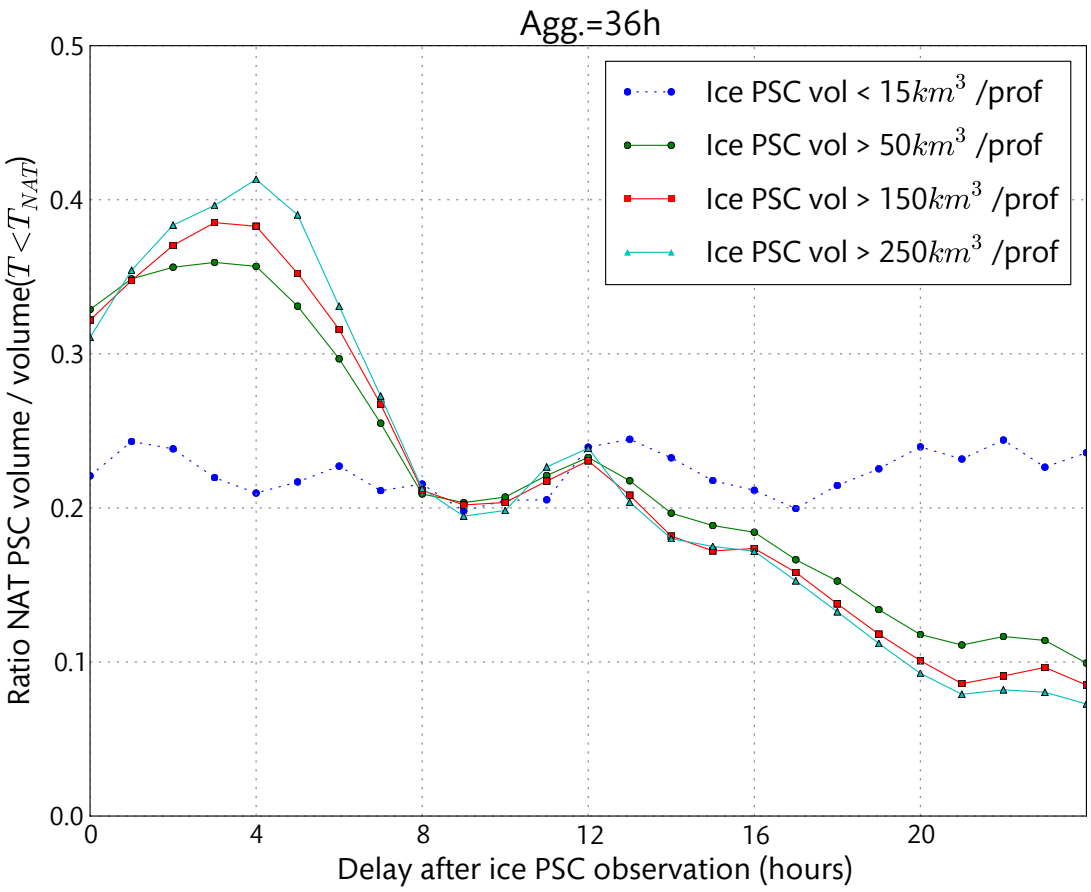

Fig. 19: Ratio of the observed volume of NAT PSC on the modeled volume of temperatures conducive to NAT PSC formation, for four ranges of observed ice PSC volumes, as a function of the delay after ice PSC observation. Volumes were aggregated over 36-hours periods with an adjustable delay between ice and NAT data.